Journal of Nuclear Medicine, published on July 9, 2020 as doi:10.2967/jnumed.120.247411

Voxel-Wise and Patient-Wise Correlation of ^{18}F-FDOPA PET, rCBV, and ADC in Treatment-Naïve Diffuse Gliomas with Different Molecular Subtypes

Authors:

Hiroyuki Tatekawa[1,2], Akifumi Hagiwara[1,2], Jingwen Yao[1,2,3], Talia C. Oughourlian[1,2,4], Issei Ueda[2], Hiroyuki Uetani[2], Catalina Raymond[1,2], Albert Lai[5,6], Timothy F. Cloughesy[5,6], Phioanh L. Nghiemphu[5,6], Linda M. Liau[5,7], Whitney B. Pope[2], Noriko Salamon[2], Benjamin M. Ellingson[1,2,3,4,5]

Affiliation:

1. UCLA Brain Tumor Imaging Laboratory, Center for Computer Vision and Imaging Biomarkers, David Geffen School of Medicine, University of California Los Angeles

2. Department of Radiological Science, David Geffen School of Medicine, University of California Los Angeles

3. Department of Bioengineering, Henry Samueli School of Engineering, University of California Los Angeles

4. Neuroscience Interdepartmental Program, David Geffen School of Medicine, University of California Los Angeles

5. UCLA Neuro-Oncology Program, David Geffen School of Medicine, University of California Los Angeles

6. Department of Neurology, David Geffen School of Medicine, University of California Los Angeles

7. Department of Neurosurgery, David Geffen School of Medicine, University of California Los Angeles

Corresponding Author:

Benjamin M. Ellingson

924 Westwood Blvd., Suite 615, Los Angeles, CA 90024

Phone:(310)481-7572/Fax:(310)794-2796

bellingson@mednet.ucla.edu

Reprints are not available.

First Author:

Hiroyuki Tatekawa

924 Westwood Blvd., Suite 615, Los Angeles, CA 90024

Phone:(310)481-7572/Fax:(310)794-2796

HTatekawa@mednet.ucla.edu

Funding/Disclosure:

SNMMI(Tatekawa); ACS Research Scholar Grant(RSG-15-003-01-CCE:Ellingson); ABTA Research Collaborators Grant(ARC1700002:Ellingson); NBTS Research Grant(Ellingson,Cloughesy); NIH/NCI UCLA Brain Tumor SPORE(1P50CA211015-01A1:Ellingson,Lai,Cloughesy,Nghiemphu); NIH/NCI(1R21CA223757-01:Ellingson)

Words:

Abstract: 251/350; Total: 5738/5000

Correlation of FDOPA and MRI for gliomas

ABSTRACT

PURPOSE To identify correlations of gliomas between ^{18}F-fluorodihydroxyphenylalanine (FDOPA) uptake and physiological magnetic resonance imaging (MRI) including relative cerebral blood volume (rCBV) and apparent diffusion coefficient (ADC) with different molecular subtypes, and to evaluate their prognostic values.

METHODS Sixty-eight treatment-naïve glioma patients who underwent FDOPA positron emission tomography (PET) and physiological MRI were retrospectively selected (isocitrate dehydrogenase wild-type [IDH_{wt}], 36; mutant 1p/19q non-codeleted [$IDH_{m\text{-}non\text{-}codel}$], 16; mutant codeleted [$IDH_{m\text{-}codel}$], 16). Fluid-attenuated inversion recovery hyperintense areas were segmented and used as regions-of-interest. For voxel-wise and patient-wise analyses, Pearson's correlation coefficients ($r_{voxel\text{-}wise}$ and $r_{patient\text{-}wise}$) between the normalized standardized uptake value (nSUV), rCBV, and ADC were evaluated. Cox regression analysis was performed to investigate the associations between the overall survival (OS) and $r_{voxel\text{-}wise}$, max/median nSUV, median CBV, or median ADC.

RESULTS For IDH_{wt} and $IDH_{m\text{-}non\text{-}codel}$ gliomas, nSUV demonstrated significant positive correlations with rCBV ($r_{voxel\text{-}wise}$ = 0.25 and 0.31, and $r_{patient\text{-}wise}$ = 0.50 and 0.70, respectively), and negative correlations with ADC ($r_{voxel\text{-}wise}$ = −0.19 and −0.19, and $r_{patient\text{-}wise}$ = −0.58 and −0.61, respectively) in both voxel-wise and patient-wise analyses. $IDH_{m\text{-}codel}$ gliomas only demonstrated a significant positive correlation between nSUV and ADC in voxel-wise analysis ($r_{voxel\text{-}wise}$ = 0.18). In Cox regression analysis, only $r_{voxel\text{-}wise}$ between nSUV and rCBV (hazard ratio [HR] = 28.82) or ADC (HR = 0.085) had significant associations with OS for IDH_{wt} gliomas.

CONCLUSION $IDH_{m\text{-}codel}$ gliomas showed distinctive patterns of correlations between amino acid PET and physiological MRI. Stronger correlations of nSUV and rCBV or ADC may result in worse prognosis for IDH_{wt} gliomas.

KEY WORDS: FDOPA PET, glioma, correlation coefficient, rCBV, ADC

INTRODUCTION

Magnetic resonance imaging (MRI) is the imaging modality of choice for clinical evaluation of gliomas due to its high spatial resolution, significant contrast in soft tissues, and a lack of ionizing radiation. Various advanced sequences to evaluate physiological status, such as perfusion imaging, diffusion-weighted imaging (DWI), spectroscopy, and functional MRI, can be readily acquired during clinical examinations. Amino acid positron emission tomography (PET), such as ^{18}F-fluorodihydroxyphenylalanine (FDOPA) and ^{18}F-fluorethyltyrosine (FET), is often used in neuro-oncological practices to identify metabolically active tumor tissues. These amino acid PETs provide information that complement MRI, and the combination of PET and MRI metrics were reported to be useful for clinical management of gliomas (*1,2*). Hybrid examinations of PET and MRI have recently been performed for evaluating gliomas in clinical practice (*3*). Hence, knowledge of their imaging features and association of their findings is instrumental for clinical treatment and predicting prognosis.

Although some previous studies have correlated amino acid PET and physiological MRI such as perfusion imaging or DWI (*4,5*), most studies demonstrated complementary and partially congruent information in PET and physiological MRI. These correlation studies often evaluated representative MRI features, including the maximum, mean, median, or minimum values, within a specific tumor region such as the contrast-enhanced or focal hypermetabolic area. However, only a few studies have evaluated the voxel-wise correlations between amino acid PET and physiological MRI within a whole tumor, the evaluation of which is unbiased. Previous voxel-wise analyses have reported a positive correlation between the FET uptake and relative cerebral blood volume (rCBV) (*6*), and a negative correlation between the FDOPA uptake and apparent diffusion coefficient (ADC) in grade III and IV gliomas (*7*). Hence, amino acid PET and physiological MRI may depict partially overlapping pathophysiological features.

In 2016, the World Health Organization (WHO) classification of tumors of the central nervous system was modified to include molecular subtypes, such as isocitrate dehydrogenase (IDH) gene mutation and chromosomal 1p/19q co-deletion, for brain tumor classification (*8*). These molecular subtypes have proven to be essential for treatment decision and prognosis. However, there have been no studies evaluating the correlations of amino acid PET with physiological MRI in different molecular subtypes, or the associations of their correlations with patient prognosis. We hypothesize that these correlations may differ among different tumor subtypes and affect prognosis. The objectives of this study were to reveal the correlations between FDOPA uptake, rCBV, and ADC in treatment-

naïve gliomas with different molecular subtypes, especially IDH mutation and 1p/19q codeletion status; and to evaluate the associations of their correlations and patient prognoses.

MATERIALS AND METHODS

Patient Selection

Sixty-eight treatment naïve and histologically confirmed glioma patients who underwent FDOPA PET and MRI scans between 2007 and 2019 were retrospectively selected. The selected MRI were acquired within 2 months of the corresponding PET images. The MRI scans consisted of at least pre- and post-contrast T1-weighted images and T2-weighted fluid-attenuated inversion recovery (FLAIR) images. Perfusion imaging for 61 subjects, and DWI for 63 subjects were obtained. The median date between PET scan and surgery or biopsy was 16 days (range, 1–505 days). No patients underwent stereotactic biopsy prior to FDOPA PET or MRI. Patients were classified by IDH mutational status and 1p/19q codeletion status, which were detected by conventional techniques (*9*). When available, O6-methylguanine-DNA methyltransferase (MGMT) promoter methylation status and epidermal growth factor receptor (EGFR) amplification status were obtained as supplementary information. The overall survival (OS) was measured from the time of the PET scans until death or the censored dates (median interval, 721 days), with 18 subjects who had deceased at the time of analysis. The study has been approved by the institutional review board, and all subjects signed an informed consent form. TABLE 1 summarizes the patient demographics and molecular information, while SUPPLEMENTAL TABLE 1 describes each patient in more detail.

Acquisition of MRI

Anatomical MRI consisted of standard T1-weighted pre- and post-contrast images (2D axial turbo spin echo with a slice thickness of 3 mm and no interslice gap, or 3D inversion prepared gradient echo images with an isotropic voxel size of 1–1.5 mm), and T2-weighted FLAIR images at a 3-mm slice thickness with no interslice gap from a 1.5-T or 3-T clinical MRI scanner.

For dynamic susceptibility contrast (DSC) perfusion MRI, a total dose of 0.1 mmol/kg of Gd-DTPA or Gd-BTDO3A (Magnevist or Gadavist; Bayer HealthCare Pharmaceuticals, Wayne, NJ) was administered with 0.025 mmol/kg of the preload dosage to mitigate T1-based leakage contamination, and the remaining 0.075 mmol/kg was

used for dynamic bolus administration as previously described (*10*). A 2-min gap was taken between the preload dose and the start of the baseline DSC-MRI. The DSC-MRI was acquired with TE/TR = 21–23/1250–1290 ms, flip angle = 60°, matrix size = 128 × 128, slice thickness = 5 mm, with no interslice gap. The number of baseline acquisitions before contrast agent injection was 10–25, and number of timepoints was 120. First, dynamic time-series images were motion-corrected using the FSL software (*mcflirt*; FMRIB, Oxford, UK; http://www.fmrib.ox.ac.uk/fsl/). Second, rCBV maps were calculated using a bidirectional contrast agent leakage-correction algorithm, to model the contrast flux into and out of the vasculature. Finally, a normalized rCBV map was computed by dividing the rCBV map by the median rCBV value of regions of interest (ROIs) placed on the contralateral normal-appearing white matter.

DWI was performed prior to the injection of the contrast agent using a single-shot echo-planar imaging sequence in the axial plane for 9 patients, and was acquired with TR/TE = 3000–10400/77–93 ms, matrix size = 128 × 128, and slice thickness = 3 mm with no interslice gap. ADC maps were calculated from the acquired DWI with b = 1000 s/mm^2 and b = 0 s/mm^2 images, and expressed in units of 10^{-6} mm^2/s. Diffusion tensor imaging (DTI) data was collected for 54 patients for whom conventional DWI was not obtained. Mean diffusivity maps were used as estimates of ADC values after motion correction using the FSL software (*dtifit*). The parameters of the DTI consisted of 12–64 equidistant diffusion-sensitizing directions with b = 1000 s/mm^2, along with a single b = 0 s/mm^2 image with TR/TE = 4500–11500/79–93 ms, matrix size = 128 × 128, and slice thickness = 2 mm with no interslice gap.

Acquisition of FDOPA PET

FDOPA PET images were acquired using a high-resolution full-ring PET scanner (ECAT-HR; CTI/MIMVista; Siemens, Knoxville, TN), after the subjects fasted for more than 4 hours. Following previously established procedures, FDOPA was synthesized and injected intravenously (*11*). Computerized tomography images were acquired prior to the PET for attenuation correction. Three-dimensional FDOPA emission data were acquired for a total of 30 min, and the data were integrated between 10–30 min following injection to obtain 20-min static FDOPA images following reconstruction. PET images were reconstructed using an ordered-subset expectation maximization iterative reconstruction algorithm, consisting of six iterations with eight subsets (*12*). Finally, a Gaussian filter with a full width at a half maximum of 4 mm was applied. The resulting voxel sizes were 1.34 mm ×

1.34 mm × 3 mm for the FDOPA PET images. Standardized uptake value (SUV) maps of FDOPA were calculated based on the radioactivity divided by the decay-corrected injected dose per body mass (*13*). The resulting SUV images were then normalized to the median value of the striatum (nSUV) as previously described (*14*).

Postprocessing and ROI Analysis

All MRI and PET images were registered to the post-contrast T1-weighted images for each patient using a 6-degree of freedom rigid transformation, and a mutual information cost function using the FSL software (*flirt*). To register the ADC maps, we rigidly aligned b = 0 s/mm^2 images acquired during the DWI or DTI sequence to the post-contrast T1-weighted images, and applied the transform matrices to the ADC maps. When needed, manual alignment was performed with the Freesurfer software (*tkregister2*; Massachusetts General Hospital, MA; https://surfer.nmr.mgh.harvard.edu). A single ROI ($FLAIR_{ROI}$) was segmented based on the hyperintense regions on the T2-weighted FLAIR by a board-certificated neuroradiologist (H.T. with 13 years of clinical experience) with the Analysis of Functional NeuroImages (AFNI) software (NIMH Scientific and Statistical Computing Core; Bethesda, MD; https://afni.nimh.nih.gov) using a semi-automatic procedure as previously described (*15*).

Statistical Analyses

The maximum nSUV, median nSUV, median rCBV, and median ADC within $FLAIR_{ROI}$ were assessed between the different molecular subtypes by one-way analysis of variance (ANOVA) and Student *t*-test, or the Kruskal-Wallis and Mann-Whitney *U* tests.

For voxel-wise analysis, nSUV, rCBV and ADC within $FLAIR_{ROI}$ were compared using the Pearson's correlation coefficients ($r_{\text{voxel-wise}}$) for each patient. The correlation coefficients were evaluated for each molecular subtype to determine whether the 95% confidential interval (CI) of mean values included zero. These correlation coefficients were also compared for the different molecular subtypes using ANOVA and Student *t*-test. In order to account for inter-individual variation, a linear mixed-effects model (fixed slope and random intercept) was also employed, given by the following equation.

$$rCBV_{im}\ (or\ ADC_{im}) = \beta_0 + \beta_1 nSUV_{im} + b_{0m} + \varepsilon_{im} \quad [1],$$

where $rCBV_{im}$ (or ADC_{im}) and $nSUV_{im}$ represents rCBV (or ADC), and FDOPA measurements of voxel *i* in patient *m*. β denotes the fixed effects, b_{0m} is the random effect for patient *m* (*i.e.* patient/acquisition-specific), and ε_{im} is the

observation error (*6*). Additionally, area under the curve (AUC) of receiver operating characteristic (ROC) curves, along with sensitivity and specificity, were analyzed to evaluate the discrimination ability of $r_{\text{voxel-wise}}$ between different molecular subtypes.

For the patient-wise analysis, Pearson's correlation coefficients ($r_{\text{patient-wise}}$) between the median nSUV, median rCBV, and median ADC were calculated. The Fisher R-to-Z transformation was used to compare the strength of $r_{\text{patient-wise}}$ between the different molecular subtypes.

Cox multivariate regression analyses controlling for age were performed to investigate the association of the OS with maximum nSUV, median nSUV, median CBV, and median ADC, as well as for $r_{\text{voxel-wise}}$ between nSUV, rCBV, and ADC. Kaplan-Meier curves and log-rank tests were employed to differentiate short- and long-term survival for gliomas stratified by the median value of the $r_{\text{voxel-wise}}$.

Statistical analysis was performed using MATLAB (R2019b; MathWorks, Natick, MA) and GraphPad Prism (Version 8.3; GraphPad Software, La Jolla, CA). Statistical significance was defined at $P < 0.05$, and no correction for multiple comparison was performed.

RESULTS

The current study included 68 treatment-naïve glioma patients (26 females) with a mean age of 51.7 years at the time of the PET examination. According to the 2007/2016 WHO criteria, 14 gliomas were grade IV, 25 were grade III, and 29 were grade II; 36 gliomas were IDH wild-type (IDH_{wt}), 16 were IDH mutant 1p/19q non-codeleted ($IDH_{m\text{-}non\text{-}codel}$), and 16 were IDH mutant 1p/19q codeleted ($IDH_{m\text{-}codel}$); 27 gliomas were MGMT unmethylated, 27 were methylated, and the remaining 14 did not have available MGMT status; 38 gliomas were EGFR amplification negative, 11 were positive, and the remaining 19 did not have available EGFR status.

FIGURE 1 illustrates an example of a segmented $FLAIR_{ROI}$ and a voxel-wise analysis between nSUV and rCBV or ADC in a 36-year-old male patient. This patient had a WHO grade IV, IDH_{wt}, MGMT unmethylated, and EGFR amplification positive glioblastoma, and showed a positive voxel-wise correlation between nSUV and rCBV, and a negative voxel-wise correlation between nSUV and ADC. The median nSUV, rCBV, and ADC within the $FLAIR_{ROI}$ were also calculated for the patient-wise analyses.

TABLE 2 shows the extracted values of the FDOPA and physiological MRI. The maximum nSUV was significantly higher in the IDH_{wt} gliomas than in the $IDH_{m\text{-}non\text{-}codel}$ gliomas ($P = 0.007$), while the median nSUV was significantly higher in the $IDH_{m\text{-}codel}$ gliomas than in the $IDH_{m\text{-}non\text{-}codel}$ gliomas ($P = 0.004$). The median rCBV was significantly higher in the IDH_{wt} gliomas than in the $IDH_{m\text{-}non\text{-}codel}$ gliomas ($P = 0.009$), while the median ADC was significantly lower in the IDH_{wt} gliomas than both the $IDH_{m\text{-}non\text{-}codel}$ ($P < 0.001$) and $IDH_{m\text{-}codel}$ gliomas ($P = 0.001$).

The IDH_{wt} and $IDH_{m\text{-}non\text{-}codel}$ gliomas demonstrated significant positive correlations between nSUV and rCBV (FIGURE 2, 3; IDH_{wt}, $r_{voxel\text{-}wise} = 0.25$, CI = [0.17, 0.32], and $r_{patient\text{-}wise} = 0.50$, CI = [0.19, 0.73]; $IDH_{m\text{-}non\text{-}codel}$, $r_{voxel\text{-}wise} = 0.31$, CI = [0.23, 0.39], and $r_{patient\text{-}wise} = 0.70$, CI = [0.33, 0.89]) in both voxel-wise and patient-wise analyses. They also exhibited significant negative correlations between nSUV and ADC (IDH_{wt}, $r_{voxel\text{-}wise} = -0.19$, CI = [−0.28, −0.10] and $r_{patient\text{-}wise} = -0.58$, CI = [−0.77, −0.30]; $IDH_{m\text{-}non\text{-}codel}$, $r_{voxel\text{-}wise} = -0.19$, CI = [−0.31, −0.06] and $r_{patient\text{-}wise} = -0.61$, CI = [−0.85, −0.15]). The $IDH_{m\text{-}codel}$ gliomas demonstrated a significant positive correlation between nSUV and ADC in the voxel-wise analysis. Other voxel-wise and patient-wise correlations between nSUV and rCBV or ADC did not show statistical significance (between nSUV and rCBV, $r_{voxel\text{-}wise} = 0.07$, CI = [−0.03, 0.16] and $r_{patient\text{-}wise} = 0.18$, CI = [−0.41, 0.66]; between nSUV and ADC, $r_{voxel\text{-}wise} = 0.18$, CI = [0.04, 0.31] and $r_{patient\text{-}wise} = 0.17$, CI = [−0.38, 0.64]). When comparing $r_{voxel\text{-}wise}$ among different molecular subtypes, the $r_{voxel\text{-}wise}$ between nSUV and rCBV was significantly lower ($p = 0.008$ and < 0.001), and the $r_{voxel\text{-}wise}$ between nSUV and ADC was significantly higher in $IDH_{m\text{-}codel}$ than in IDH_{wt} and $IDH_{m\text{-}non\text{-}codel}$ gliomas (both $Ps < 0.001$). When comparing the strengths of the patient-wise correlation coefficient among the different molecular subtypes, there were no significant differences in the $r_{patient\text{-}wise}$ between the median nSUV and rCBV (all $Ps > 0.09$). The patient-wise correlation between the median nSUV and ADC was significantly weaker in $IDH_{m\text{-}codel}$ than in IDH_{wt} ($P = 0.016$) and $IDH_{m\text{-}non\text{-}codel}$ ($P = 0.032$). Because grade IV gliomas were included only in the IDH_{wt} group, voxel-wise and patient-wise analyses were performed on only lower-grade IDH_{wt} gliomas (grade II and III; n = 22). The lower-grade IDH_{wt} cohort exhibited similar voxel-wise trends as the IDH_{wt} group including all grades. However, no significant patient-wise correlation between nSUV and rCBV was observed (IDH_{wt} with lower grade, between nSUV and rCBV, $r_{voxel\text{-}wise} = 0.22$, CI = [0.12, 0.31], and $r_{patient\text{-}wise} = 0.35$, CI = [−0.11, 0.68]; between nSUV and ADC, $r_{voxel\text{-}wise} = -0.14$, CI = [−0.27, −0.01], and $r_{patient\text{-}wise} = -0.54$, CI = [−0.80, −0.13]). The voxel-wise and patient-wise analyses between rCBV and ADC are described in SUPPELENTAL FIGURE 1.

In a linear mixed effect model (SUPPLEMENTAL TABLE 2), the mean slope (β_1) for the prediction of rCBV by nSUV (fixed effects) were 1.24, 2.52, and 0.76 in IDH_{wt}, $IDH_{m\text{-}non\text{-}codel}$, and $IDH_{m\text{-}codel}$, respectively. The mean slope (β_1) for the prediction of ADC by nSUV were −157, −649, and 187 in IDH_{wt}, $IDH_{m\text{-}non\text{-}codel}$, and $IDH_{m\text{-}codel}$, respectively. All slopes (β_1) of the mixed effect model were consistent with the voxel-wise and patient-wise analyses.

The ROC analysis differentiated $IDH_{m\text{-}codel}$ from IDH_{wt} and $IDH_{m\text{-}non\text{-}codel}$ gliomas with AUC, sensitivity, and specificity of 0.80, 63%, and 92%, respectively, for $r_{voxel\text{-}wise}$ between nSUV and rCBV; 0.86, 76%, and 86%, respectively, for $r_{voxel\text{-}wise}$ between nSUV and ADC; and 0.68, 69%, and 73%, respectively, for $r_{voxel\text{-}wise}$ between rCBV and ADC (FIGURE 4). The differentiation between IDH_{wt} and IDH_m gliomas is shown in SUPPLEMENTAL FIGURE 2.

Because no patients in $IDH_{m\text{-}non\text{-}codel}$ and only one patient in $IDH_{m\text{-}codel}$ gliomas had deceased, only the IDH_{wt} gliomas (n = 36) were included in the Cox regression analysis and log-rank test. The Cox multivariate analysis controlling for age (TABLE 3) demonstrated significant associations in hazard with the $r_{voxel\text{-}wise}$ between nSUV and rCBV (hazard ratio [HR] = 28.82, $P = 0.017$), and between nSUV and ADC (HR = 0.085, $P = 0.038$). The significant associations did not change when controlling for age and surgical procedure (resection or biopsy) (data not shown). The Kaplan-Meier curves and log-rank tests showed a significant difference in the OS ($P = 0.049$) when IDH_{wt} gliomas were stratified by the median value of the $r_{voxel\text{-}wise}$ between nSUV and ADC, with lower $r_{voxel\text{-}wise}$ associated with worse survival (SUPPLEMENTAL FIGURE 3).

The voxel-wise and patient-wise analyses between different MGMT methylation statuses or between different EGFR amplification statuses are summarized in SUPPELENTAL FIGURE 4, 5, and SUPPELENTAL TABLE 3, 4.

DISCUSSION

In this study, voxel-wise and patient-wise correlations between FDOPA uptake, rCBV, and ADC were evaluated among different molecular subtypes. For IDH_{wt} and $IDH_{m\text{-}non\text{-}codel}$ gliomas, nSUV and rCBV had significant positive correlations, while nSUV and ADC had significant negative correlations. In contrast, $IDH_{m\text{-}codel}$ gliomas demonstrated a significant positive correlation between nSUV and ADC in the voxel-wise analysis, which

was an inverse relationship identified in IDH_{wt} or $IDH_{m\text{-}non\text{-}codel}$ gliomas. No other correlations in $IDH_{m\text{-}codel}$ gliomas showed statistical significance. The $r_{voxel\text{-}wise}$ could discriminate $IDH_{m\text{-}codel}$ from $IDH_{m\text{-}non\text{-}codel}$ gliomas with high accuracy (AUC = 0.88 for $r_{voxel\text{-}wise}$ between nSUV and ADC). The Cox regression analysis revealed that the $r_{voxel\text{-}wise}$ between nSUV and rCBV or ADC had a significant association with OS for IDH_{wt} gliomas.

Results from the current study suggest that the physiological features of $IDH_{m\text{-}codel}$ gliomas may be different from those of IDH_{wt} or $IDH_{m\text{-}non\text{-}codel}$ gliomas. In the 2016 WHO classification of tumors of the central nervous system, oligodendrogliomas are defined by the presence of both IDH mutation and 1p/19q codeletion (*8*). IDH mutant 1p/19q codeleted oligodendrogliomas showed higher amino acid tracer uptake, higher rCBV, and lower ADC, compared with IDH mutant 1p/19q non-codeleted diffuse astrocytomas (*16*). These physiological imaging features are compatible with our results, although some results were not statistically significant. The uptake of amino acid tracers in oligodendrogliomas is known to reflect transportation mediated by amino acid carriers over the endothelial cell membrane, and to correlate with microvessel and cell density of the tumor (*17*). The presence of a branching network of delicate capillaries (chicken-wire pattern) or the frequent cortical involvement of oligodendrogliomas relative to astrocytomas may cause relatively higher rCBV (*18-20*). Oligodendrogliomas are often highly cellular in the central regions with closely packed, relatively small cells (*18*), which may result in relatively lower ADC. These pathological features and anatomical localization may reflect the physiological imaging features of oligodendrogliomas.

However, in less cellular areas at the periphery of oligodendrogliomas, diffuse infiltrative growth can be pathologically easily identified, often with prominent secondary structure formation, including clustering of tumor cells around the perikarya of pre-existing neurons under the pial surface, and surrounding cortical small vessels (*18*). A previous voxel-wise histogram analysis also reported higher vascular heterogeneity in oligodendrogliomas compared to astrocytomas (*16*). Such intra-tumoral, diverse, and heterogeneous pathological features of oligodendrogliomas may have resulted in an inverse correlation to other gliomas or no correlations between FDOPA uptake and rCBV or ADC.

In the current study, the $r_{voxel\text{-}wise}$ between nSUV and rCBV or ADC had a significant association with OS in IDH_{wt} gliomas. Gross tumor heterogeneity shown by histogram and texture analyses of PET have been suggested to be associated with survival of patients with gliomas (*21,22*). However, the results of these studies were incongruent in terms of gross tumor heterogeneity, and it was difficult to understand the microstructural underpinnings: higher

contrast and busyness, indicating higher heterogeneity, were associated with worse survival; on the contrary, higher kurtosis and coarseness, indicating less heterogeneity, were associated with worse survival. In contrast, to the best of our knowledge, our study is the first to show the contribution of voxel-level heterogeneity to survival. Cell proliferation, development, and maintenance with an adequate blood supply by angiogenesis are essential for tumor growth and invasion (*17,23,24*). Previous imaging pathological correlation studies have shown that rCBV was associated with tumor cell density (*23*), tumor proliferation (*25*), and vascularization (*26*). Regions with low ADC were also reported to reflect a high mitotic index and tumor cell density (*7*). In these areas, hypermetabolism indicated by amino acid PET might reflect an accelerated and efficient tumor growth cycle. In contrast, gliomas with co-existing normal central nervous system cells, large extracellular space, or abundant macro-molecules such as proteoglycans and adhesion protein, may reflect heterogeneous pathological features (*5,27*). Gliomas with such heterogeneous features may be associated with weak correlations between physiological MRI/PET, less efficient growth, and better prognosis.

The current study had some limitations and future directions. First, not all MRI scans were performed using the same acquisition parameters and scanners. Further, differences in patient age and sex may also have affected the FDOPA uptake (*28*); however, our approach is supported by the results of the mixed effect model, which accounts for inter-individual variation and demonstrates consistent results with the voxel-wise and patient-wise correlation analyses. Second, because associations of the imaging correlations and pathological features were not confirmed, a stereotactic image-histology comparison may be required in a future study. Third, only FLAIR hyperintense ROIs were used for the voxel-wise and patient-wise analyses, while the ROIs of contrast enhancement were not used. This is because only one-third of the patients (70% of them were IDH_{wt}) showed contrast enhancement. Furthermore, only the IDH_{wt} group was included in the Cox regression analysis. A study with a larger population including all subtypes or those other than IDH_{wt} may reveal new biomarkers of gliomas. Fourth, although Karnofsky Performance Status is an important factor to evaluate survival, the status was not available for all subjects, and thus not analyzed in this study. Finally, the existence of necrosis, hemorrhage, and calcification were not considered in this study. If necrosis exists in a tumor, both FDOPA uptake and rCBV are expected to decrease and ADC is expected to increase. Hence, necrosis may enhance the strengths of correlation coefficients between FDOPA and rCBV or ADC by increasing the range of these metrics. However, hemorrhage may change ADC values over time due to the change in ratio of oxy/deoxy-hemoglobin and hemosiderin. Furthermore, hemosiderin deposition and dense calcification lead

to very low ADC value. Although no data were excluded in this study, elimination of outliers in ADC values may increase the prediction performance.

CONCLUSION

In the voxel-wise and patient-wise analyses, IDH_{wt} and $IDH_{m\text{-}non\text{-}codel}$ gliomas showed significant positive correlations between FDOPA uptake and rCBV, and significant negative correlations between the FDOPA uptake and ADC. In contrast, $IDH_{m\text{-}codel}$ gliomas had either an inverse correlation to other glioma subtypes, or no significant correlations between FDOPA uptake and rCBV or ADC, which may reflect the unique pathological features of heterogeneous or diverse oligodendroglial components. A strong correlation of the FDOPA uptake and rCBV or ADC in IDH_{wt} may contribute to the acceleration of efficient and aggressive tumor growth, resulting in worse prognosis.

KEY POINTS

Question: The correlation of FDOPA PET and physiological MRI in different molecular subtypes is unrevealed.

Pertinent findings: This cohort study reveals specific correlations patterns between FDOPA PET and physiological MRI in different molecular subtypes.

Implication for patient care: Correlation of FDOPA PET and physiological MRI may predict prognosis

DISCLOSURE

SNMMI (HT); ACS Research Scholar Grant (RSG-15-003-01-CCE: BME); ABTA Research Collaborators Grant (ARC1700002: BME); NBTS Research Grant (BME,TFC); NIH/NCI UCLA Brain Tumor SPORE (1P50CA211015-01A1: BME, AL, TFC, PLN); NIH/NCI (1R21CA223757-01: BME)

BME is an advisor for Hoffman La-Roche; Siemens; Nativis; Medicenna; MedQIA; Bristol Meyers Squibb; Imaging Endpoints; and Agios Pharmaceuticals. BME is a Paid Consultant for Nativis; MedQIA; Siemens; Hoffman La-Roche; Imaging Endpoints; Medicenna; and Agios. BME received grant funding from Siemens, Agios, and

Janssen. TFC is on the advisory board for Roche/Genentech, Amgen, Tocagen, NewGen, LPath, Proximagen, Celgene, Vascular Biogenics Ltd, Insys, Agios, Cortice Bioscience, Pfizer, Human Longevity, BMS, Merck, Notable Lab, and MedQIA. No other potential conflicts of interest relevant to this article exist.

REFERENCES

1. Galldiks N, Lohmann P, Cicone F, Langen KJ. FET and FDOPA PET imaging in glioma. In: Pope W, ed. *Glioma Imaging*. 1st ed. Switzerland: Springer; 2019:211-222.

2. Verburg N, Koopman T, Yaqub MM, et al. Improved detection of diffuse glioma infiltration with imaging combinations: a diagnostic accuracy study. *Neuro Oncol.* 2020;22:412-422.

3. Deuschl C, Kirchner J, Poeppel TD, et al. (11)C-MET PET/MRI for detection of recurrent glioma. *Eur J Nucl Med Mol Imaging.* 2018;45:593-601.

4. Rossi Espagnet MC, Romano A, Mancuso V, et al. Multiparametric evaluation of low grade gliomas at follow-up: comparison between diffusion and perfusion MR with (18)F-FDOPA PET. *Br J Radiol.* 2016;89:20160476.

5. Rahm V, Boxheimer L, Bruehlmeier M, et al. Focal changes in diffusivity on apparent diffusion coefficient MR imaging and amino acid uptake on PET do not colocalize in nonenhancing low-grade gliomas. *J Nucl Med.* 2014;55:546-550.

6. Gottler J, Lukas M, Kluge A, et al. Intra-lesional spatial correlation of static and dynamic FET-PET parameters with MRI-based cerebral blood volume in patients with untreated glioma. *Eur J Nucl Med Mol Imaging.* 2017;44:392-397.

7. Karavaeva E, Harris RJ, Leu K, et al. Relationship between [18F]FDOPA PET uptake, apparent diffusion coefficient (ADC), and proliferation rate in recurrent malignant gliomas. *Mol Imaging Biol.* 2015;17:434-442.

8. Louis DN, Perry A, Reifenberger G, et al. The 2016 World Health Organization classification of tumors of the central nervous system: a summary. *Acta Neuropathol.* 2016;131:803-820.

9. Oughourlian TC, Yao J, Schlossman J, et al. Rate of change in maximum (18)F-FDOPA PET uptake and non-enhancing tumor volume predict malignant transformation and overall survival in low-grade gliomas. *J Neurooncol.* 2020;147:135-145.

10. Leu K, Boxerman JL, Lai A, et al. Bidirectional contrast agent leakage correction of dynamic susceptibility contrast (DSC)-MRI improves cerebral blood volume estimation and survival prediction in recurrent glioblastoma treated with bevacizumab. *J Magn Reson Imaging.* 2016;44:1229-1237.

11. Namavari M, Bishop A, Satyamurthy N, Bida G, Barrio JR. Regioselective radiofluorodestannylation with [18F]F2 and [18F]CH3COOF: a high yield synthesis of 6-[18F]Fluoro-L-dopa. *Int J Rad Appl Instrum A.* 1992;43:989-996.

12. Nuyts J, Michel C, Dupont P. Maximum-likelihood expectation-maximization reconstruction of sinograms with arbitrary noise distribution using NEC-transformations. *IEEE Trans Med Imaging.* 2001;20:365-375.

13. Thie JA. Understanding the standardized uptake value, its methods, and implications for usage. *J Nucl Med.* 2004;45:1431-1434.

14. Chen W, Silverman DH, Delaloye S, et al. 18F-FDOPA PET imaging of brain tumors: comparison study with 18F-FDG PET and evaluation of diagnostic accuracy. *J Nucl Med.* 2006;47:904-911.

15. Ellingson BM, Kim HJ, Woodworth DC, et al. Recurrent glioblastoma treated with bevacizumab: contrast-enhanced T1-weighted subtraction maps improve tumor delineation and aid prediction of survival in a multicenter clinical trial. *Radiology.* 2014;271:200-210.

16. Latysheva A, Emblem KE, Brandal P, et al. Dynamic susceptibility contrast and diffusion MR imaging identify oligodendroglioma as defined by the 2016 WHO classification for brain tumors: histogram analysis approach. *Neuroradiology.* 2019;61:545-555.

17. Roodakker KR, Alhuseinalkhudhur A, Al-Jaff M, et al. Region-by-region analysis of PET, MRI, and histology in en bloc-resected oligodendrogliomas reveals intra-tumoral heterogeneity. *Eur J Nucl Med Mol Imaging.* 2019;46:569-579.

18. Wesseling P, van den Bent M, Perry A. Oligodendroglioma: pathology, molecular mechanisms and markers. *Acta Neuropathol.* 2015;129:809-827.

19. Leu K, Ott GA, Lai A, et al. Perfusion and diffusion MRI signatures in histologic and genetic subtypes of WHO grade II-III diffuse gliomas. *J Neurooncol.* 2017;134:177-188.

20. Guo H, Kang H, Tong H, et al. Microvascular characteristics of lower-grade diffuse gliomas: investigating vessel size imaging for differentiating grades and subtypes. *Eur Radiol.* 2019;29:1893-1902.

21. Pyka T, Gempt J, Hiob D, et al. Textural analysis of pre-therapeutic [18F]-FET-PET and its correlation with tumor grade and patient survival in high-grade gliomas. *Eur J Nucl Med Mol Imaging.* 2016;43:133-141.

22. Mitamura K, Yamamoto Y, Kudomi N, et al. Intratumoral heterogeneity of (18)F-FLT uptake predicts proliferation and survival in patients with newly diagnosed gliomas. *Ann Nucl Med.* 2017;31:46-52.

23. Sadeghi N, D'Haene N, Decaestecker C, et al. Apparent diffusion coefficient and cerebral blood volume in brain gliomas: relation to tumor cell density and tumor microvessel density based on stereotactic biopsies. *AJNR Am J Neuroradiol.* 2008;29:476-482.

24. Fischer I, Gagner JP, Law M, Newcomb EW, Zagzag D. Angiogenesis in gliomas: biology and molecular pathophysiology. *Brain Pathol.* 2005;15:297-310.

25. Price SJ, Green HA, Dean AF, Joseph J, Hutchinson PJ, Gillard JH. Correlation of MR relative cerebral blood volume measurements with cellular density and proliferation in high-grade gliomas: an image-guided biopsy study. *AJNR Am J Neuroradiol.* 2011;32:501-506.

26. Hu LS, Eschbacher JM, Dueck AC, et al. Correlations between perfusion MR imaging cerebral blood volume, microvessel quantification, and clinical outcome using stereotactic analysis in recurrent high-grade glioma. *AJNR Am J Neuroradiol.* 2012;33:69-76.

27. Sadeghi N, Camby I, Goldman S, et al. Effect of hydrophilic components of the extracellular matrix on quantifiable diffusion-weighted imaging of human gliomas: preliminary results of correlating apparent diffusion coefficient values and hyaluronan expression level. *AJR Am J Roentgenol.* 2003;181:235-241.

28. Cicone F, Carideo L, Minniti G, Scopinaro F. The mean striatal (18)F-DOPA uptake is not a reliable cut-off threshold for biological tumour volume definition of glioma. *Eur J Nucl Med Mol Imaging.* 2019;46:1051-1053.

FIGURES:

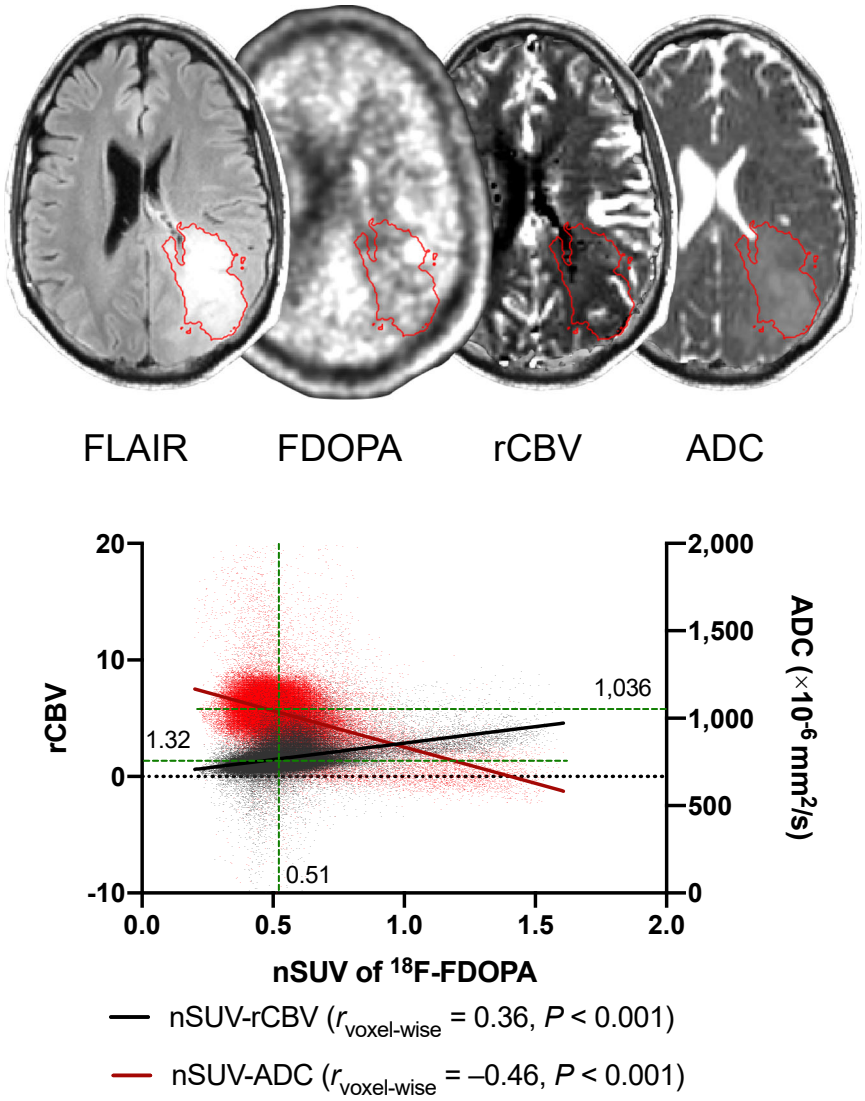

FIGURE 1 An example of postprocessing and segmentation. A 36-year-old male with treatment-naïve WHO grade IV, IDH_{wt}, MGMT unmethylated, and EGFR amplified glioblastoma. ROIs of the FLAIR hyperintense region are overlaid on the FDOPA, rCBV, and ADC maps. A scatterplot extracted from the ROI is shown with voxel-wise Pearson's correlation coefficients between nSUV and rCBV (dots and a solid line in black) or ADC (dots and solid line in red). Median nSUV, CBV, and ADC (green dot lines) are also shown

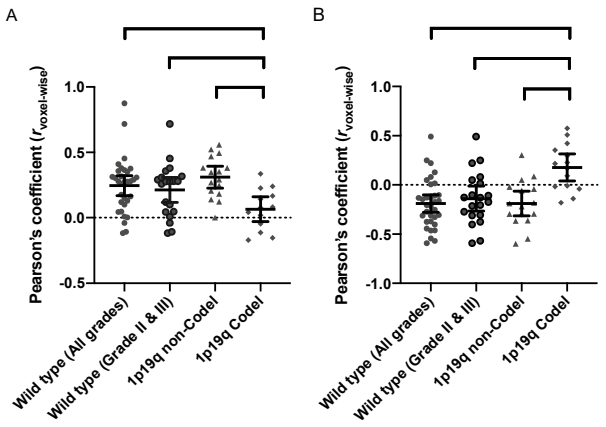

FIGURE 2 Voxel-wise Pearson's correlation coefficients A) between nSUV and rCBV and B) between FDOPA uptake and ADC. All comparisons with ANOVA are *Ps* < 0.002. Bars denote the mean value and 95% confidential interval. *, **, and *** mean *P* < 0.05, < 0.01, and < 0.001, respectively.

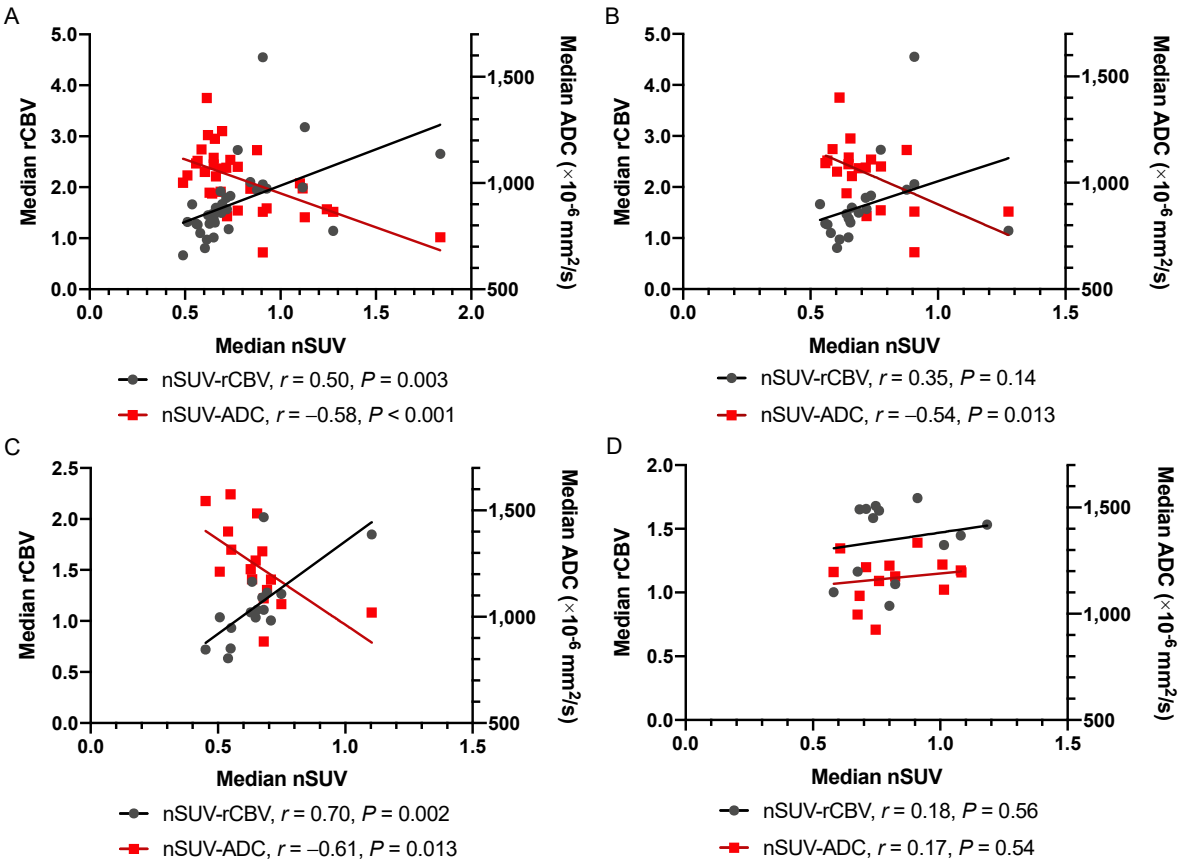

FIGURE 3 Patient-wise Pearson's correlation coefficients between the median nSUV and rCBV (black) or ADC (red) in A) IDH_{wt} (all grades), B) IDH_{wt} (grade II and III), C) $IDH_{m\text{-}non\text{-}codel}$, and D) $IDH_{m\text{-}codel}$. There are no significant differences in the strength of correlation coefficients of the median nSUV and rCBV among different molecular subtypes. The correlation coefficient of the median nSUV and ADC is significantly weaker in $IDH_{m\text{-}codel}$ than IDH_{wt} (all grades, $P = 0.016$; grade II and III, $P = 0.042$) and $IDH_{m\text{-}non\text{-}codel}$ ($P = 0.032$).

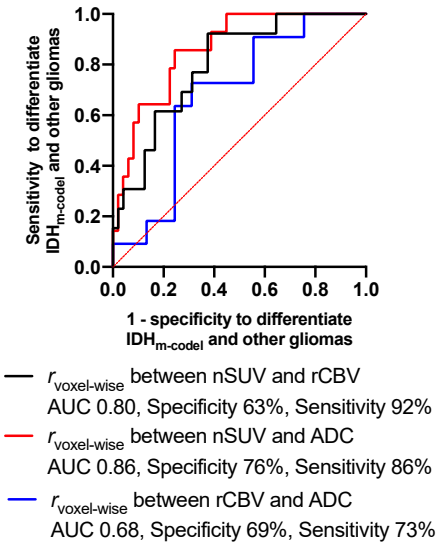

FIGURE 4 Receiver operating characteristic curve to differentiate $IDH_{m\text{-}codel}$ from IDH_{wt} and $IDH_{m\text{-}non\text{-}codel}$ gliomas.

TABLES

TABLE 1 Patient demographics and molecular information

No. of patients		68
Female		26 (38.2%)
Age ± standard deviation (year)		51.7 ± 14.9
WHO classification grade	II	29 (42.6%)
	III	25 (36.8%)
	IV	14 (20.6%)
IDH mutation and 1p/19q codeletion status	Wild-type	36 (52.9%)
	Mutant 1p/19q non-codeleted	16 (23.5%)
	Mutant 1p/19q codeleted	16 (23.5%)
MGMT-promoter methylation status	Unmethylated	27 (39.7%)
	Methylated	27 (39.7%)
	Unknown	14 (20.6%)
EGFR amplification status	Negative	38 (55.9%)
	Positive	11 (16.2%)
	Unknown	19 (27.9%)
Surgical procedure	Biopsy	12 (17.6%)
	Subtotal resection	44 (64.7%)
	Gross total resection	12 (17.6%)

IDH = isocitrate dehydrogenase; MGMT = O6-methylguanine-DNA methyltransferase; EGFR = epidermal growth factor receptor

TABLE 2 Values of FDOPA PET and physiologic MRI in IDH_{wt}, $IDH_{m\text{-}non\text{-}codel}$, and $IDH_{m\text{-}codel}$ gliomas

Tumor type	IDH_{wt}	$IDH_{m\text{-}non\text{-}codel}$	$IDH_{m\text{-}codel}$	*P* value			
				ANOVA	IDH_{wt} vs. $IDH_{m\text{-}non\text{-}codel}$	IDH_{wt} vs. $IDH_{m\text{-}codel}$	$IDH_{m\text{-}non\text{-}codel}$ vs. $IDH_{m\text{-}codel}$
Maximum nSUV	1.64 ± 0.75	1.15 ± 0.30	1.56 ± 0.92	0.024*†	0.007*‡	0.46‡	0.07‡
Median nSUV	0.78 ± 0.27	0.65 ± 0.15	0.83 ± 0.19	0.012*	0.08	0.48	0.004*
Median rCBV	1.70 ± 0.76	1.15 ± 0.37	1.42 ± 0.29	0.014*	0.009*	0.2	0.43
Median ADC ($\times 10^{-6}$ mm^2/s)	1015 ± 152	1241 ± 193	1169 ± 110	< 0.001*	< 0.001*	0.001*	0.22

Data were mean ± standard deviation; * means statistically significant; † uses Kruskal-Wallis test; ‡ uses Mann-Whitney *U* test
IDH = isocitrate dehydrogenase; wt = wild-type; m-non-codel = mutant 1p19q non-codeleted; m-codel = mutant 1p19q codeleted; nSUV = normalized standardized uptake value; rCBV = relative cerebral blood volume; ADC = apparent diffusion coefficient

TABLE 3 Cox multivariate regression controlling for age in IDH wild-type

	Hazard ratio	95% confidence interval	*P* value
Maximum nSUV	1.341	[0.737, 2.443]	0.33
Median nSUV	0.83	[0.109, 6.342]	0.86
Median rCBV	1.184	[0.666, 2.104]	0.56
Median ADC ($\times 10^{-6}$ mm^2/s)	0.998	[0.995, 1.002]	0.33
$r_{voxel\text{-}wise}$ between nSUV and rCBV	28.82	[1.828, 454.4]	0.017*
$r_{voxel\text{-}wise}$ between nSUV and ADC	0.085	[0.008, 0.874]	0.038*
$r_{voxel\text{-}wise}$ between rCBV and ADC	0.099	[0.005, 1.970]	0.13

* means statistically significant; nSUV = normalized standardized uptake value; rCBV = relative cerebral blood volume (rCBV); ADC = apparent diffusion coefficient